Data-driven Security Control for Unknown Nonlinear MASs with Hybrid Faults: A Hierarchical Control Approach

Yuyang Zhao[a], Dawei Gong[a], Jiaoyuan Chen[a], Shijie Song[b], Minglei Zhu[b]

[a]*School of Mechanical and Electrical Engineering, University of Electronic Science and Technology of China, No.2006, Xiyuan Ave, West Hi-Tech.Zone, Chengdu, 611731, Sichuan, China*

[b]*The Institute of Smart City and Intelligent Transportation, Southwest Jiaotong University, No. 999, Xi'an Road, Pidu District, Chengdu, 611756, Sichuan, China*

Abstract

In this paper, a novel hierarchical data-driven consensus control strategy is developed for unknown nonlinear multi-agent systems (MASs) subject to hybrid faults. Unlike conventional model-free adaptive control (MFAC) methods that rely on consensus errors, the proposed approach introduces a hierarchical framework that structurally decouples the control process, thereby enhancing robustness and scalability. First, a fully distributed observer is employed to estimate the leader's dynamics based solely on locally available real-time input–output measurements, without relying on any prior knowledge of the system model. Then, a distributed MFAC-based controller is designed and embedded with an online actuator fault estimation mechanism to handle unknown faults in real time. This hierarchical design enables each agent to operate independently, reduces inter-agent interference, and streamlines the adjustment of controller parameters. Moreover, theoretical analysis ensures that all estimation and tracking errors remain uniformly bounded under hybrid fault conditions. Finally, simulation studies on two numerical MAS examples and multi-manipulator platforms demonstrate the effectiveness and practical applicability of the proposed method.

Keywords:
Hierarchical Control framework, Security Control, Multi-agent Systems, Data-driven Control, Adaptive Control.

1. Introduction

Recently, cooperative control problems of multi-agent systems (MASs) have attracted significant attention due to their wide applicability in areas such as multi-robot coordination[1], autonomous vehicle formations[2], and distributed sensor networks[3]. Among these, the consensus control problem has emerged as a fundamental research topic and has been extensively studied. The primary objective of consensus control is to design distributed control laws that ensure all agents converge to a common output. Although numerous model-based approaches have been proposed to address this problem[4, 5], it is important to recognize that, in practical applications, accurately obtaining system models for each agent in the MAS is often challenging. Therefore, the development of data-driven consensus control protocols is of considerable importance.

Model-free adaptive control (MFAC) is a widely recognized online data-driven control algorithm that derives adaptive control laws from data models constructed via the dynamic linearization method[6, 7, 8, 9, 10]. Unlike other data-driven approaches, such as reinforcement learning-based methods [11], fuzzy-logic-based algorithms [12], and neural network-based algorithms [13], MFAC-based algorithms circumvent the need for prior datasets to train approximators for system dynamics modeling, enabling immediate implementation using solely real-time input–output data. In recent decades, MFAC-based algorithms have been extended to address the consensus control problem in MASs [14, 15, 16]. A distributed MFAC-based algorithm was first introduced in [17] to solve the consensus problem in MASs. The work in [18] focused on the asymmetric bipartite consensus tracking problem, while [19] presented a fully distributed data-driven control algorithm within the MFAC framework. It is worth noting that most of the aforementioned MFAC approaches for multi-agent consensus control are fundamentally based on the use of consensus errors. While this design simplifies the control structure to some extent, it also introduces notable challenges when applied to large-scale or real-time systems. The key issue lies in the fact that consensus errors do not offer the predictive output information required by MFAC algorithms, which compromises their responsiveness and adaptability in dynamic environments. Furthermore, the dependence on inter-agent consensus data induces strong coupling among agents, resulting in increased system complexity and greater difficulty in tuning control parameters as the number of agents grows.

On the other hand, most existing studies assume ideal, fault-free conditions, which is often unrealistic due to factors like component aging, hardware degradation, and environmental disturbances. These faults can severely impact control performance and system stability. Hence, developing an MFAC-based security control method that can handle such faults is essential. To the best of our knowledge, limited research has been conducted on the consensus problem in MASs with system faults under the MFAC framework. The MFAC-based control approach was first utilized in [20] to address sensor saturation, a common type of system fault. Subsequently, this approach was further developed to address the containment control problem and the formation control problem in [21] and [22], respectively. In [23], an MFAC-based control algorithm incorporating an adaptive fault estimator was proposed to address the consensus problem in MASs subject to actuator faults. Whereas most previous studies concentrate on individual fault types, the present work addresses the more complex and practically relevant scenario involving hybrid faults, which imposes greater challenges on both system analysis and controller design. In addition, it should be noted that these existing methods are generally based on consensus errors. Under such schemes, a fault occurring in a single agent can propagate through the network and adversely affect the control performance of other agents, thereby undermining the overall robustness of the system. A critical step toward overcoming these challenges is to design control schemes that eliminate the dependence on consensus errors.

Hierarchical control is a widely adopted framework for addressing cooperative control problems in heterogeneous MASs, typically comprising distributed observers and decentralized controllers. In this framework, distributed observers are employed to estimate the leader's trajectory or state, while decentralized controllers are designed to enable the followers to track the estimated trajectory or state. As a result, all agents in the hierarchical control framework have access to the leader's state, eliminating the need for consensus errors. In recent years, there have been several advances in hierarchical control research [24, 25, 26, 27, 28]. Specifically, [25] proposes novel distributed observers that rely on partially known information about leader dynamics to estimate the leader's state. Furthermore, by exploiting the universal approximation capability of neural networks (NNs), NN-based observers were developed in [26, 27, 28] to approximate the leader's dynamics and estimate its state in an online fashion. Despite these developments, several limitations persist. Most notably, traditional hierarchical control frameworks often rely on partial system knowledge or extensive offline data to

design observers, which limits their applicability in scenarios that demand fully online estimation without prior model information. In addition, the introduction of observers increases the structural complexity of the control system, making the associated stability analysis more intricate.

Motivated by the above discussion, this paper proposes a novel distributed data-driven security control algorithm based on the hierarchical control framework to address the consensus control problem in unknown nonlinear MASs subject to actuator faults and sensor saturation. The major contributions of this work are summarized as follows:

1) A novel distributed MFAC-based security control scheme is developed within a hierarchical control framework. Compared to existing MFAC-based control approaches [14, 15, 16, 17, 18], the proposed method incorporates a hierarchical structure to eliminate the reliance on consensus errors in distributed controller design. By leveraging the hierarchical framework, the entire MAS is effectively decoupled in terms of controller design, thereby reducing the propagation of errors that occur in individual agents and mitigating their impact on the overall control performance of other agents.

2) An observer-based fault-tolerant consensus control strategy is proposed to handle hybrid faults in MASs. Unlike existing MFAC-based approaches [20, 21, 22, 23] that typically consider only a single type of fault, the proposed method accounts for the simultaneous occurrence of actuator faults and sensor saturation, which introduces additional challenges in controller design. To address this, a distributed data-driven observer is introduced to predict the leader's next-step state using only local real-time information. This predictive information is then integrated into the design of both an adaptive fault estimator and a fault-tolerant controller within the MFAC framework, thereby streamlining the design of fault-tolerant controllers and enhancing the system's robustness under mixed fault conditions.

3) Different from the traditional MFAC-based control algorithm [7, 8, 9, 10, 17, 18, 19, 20, 21, 22, 23], the proposed algorithm introduces distributed observers to facilitate the use of local neighborhood errors at different time instances for controller design. This innovation allows the relaxation of the commonly imposed assumption in traditional MFAC

algorithms that the reference signal must remain constant during stability analysis, thereby enhancing the flexibility and applicability of MFAC in dynamic environments.

This paper is organized as follows. In Section II, the foundational concepts of graph theory and the security control problem are presented. In Section III, the design of distributed observers and the security controller is introduced. In Section IV, the stability analysis is provided. Section V gives three simulations to verify the effectiveness of the proposed algorithm. Finally, Section VI concludes the paper.

2. Preliminaries And Problem Formulation

2.1. Graph Theory

A weighted graph $\mathscr{G}(\mathscr{V}, \mathscr{E}, \mathscr{A})$ is applied to describe the relationship among multiple agents. Where $\mathscr{V} = \{v_1, v_2, \cdots, v_M\}$, $\mathscr{E} \subset \mathscr{V} \times \mathscr{V}$ and $\mathscr{A} = [a_{ij}] \in \mathbb{R}^{M \times M}$ denote the set of the nodes, the set of the edges and the adjacency matrix in the graph, respectively. The flow of the information is defined as a_{ij} and which satisfies $a_{ij} > 0$ if the edge $(v_i, v_j) \in \mathscr{E}$, otherwise $a_{ij} = 0$. $\mathcal{N}_i = \{v_j : (v_i, v_j) \in \mathscr{E}\}$ denotes the set of the neighbors of the node i, which can obtain the information from node i. If there is a sequence of successive edges satisfying $\{(v_i, v_c), (v_c, v_d), \cdots, (v_e, v_k)\}$, which means there is a direct path from node i to node k. A graph is said to have a spanning tree if there exists a direct path from a node to every node in the graph. The diagonal matrix $W = \text{diag}(\omega_{i0})$ denotes the weight between the followers and the leader. If the follower is the neighbor of the leader, $\omega_{i0} > 0$, else $\omega_{i0} = 0$.

Assumption 1. *[29][30] The graph $\mathscr{G}$ contains at least one spinning tree and the leader is pinned to at least one root node.*

2.2. Problem Formulation

Consider the fully heterogeneous nonlinear MASs with $\mathcal{N}$ followers and one leader, the ith follower's dynamics with actuator faults is defined as:

$$y_i(s+1) = f_i(y_i(s), u_i(s), u_{fi}(s)), \tag{1}$$

where $y_i(s) \in \mathbb{R}^{n_i}$, $u_i(s), u_{fi}(s) \in \mathbb{R}^{l_i}$ are the output, input, and actuator fault of the ith follower, and $f_i(\cdot) \in \mathbb{R}^{n_i}$ represents the unknown dynamics.

The dynamic of the leader agent is defined as:

$$x_0(s+1) = \mathcal{A}_0 x_0(s), \quad y_0(s) = \mathcal{C}_0 x_0(s), \tag{2}$$

where $x_0(s)\in\mathbb{R}^{n_0}$, $y_0(s)\in\mathbb{R}^{m_0}$, $\mathcal{A}_0\in\mathbb{R}^{n_0\times n_0}$ and $C_0\in\mathbb{R}^{m_0\times n_0}$ denote the leader's state, output, internal dynamics and output dynamics, respectively.

Assumption 2. *[31] All eigenvalues of $\mathcal{A}_0$ satisfy $|\lambda(\mathcal{A}_0)| \leq 1$.*

3. Data-driven Hierarchical Control Algorithm Design

3.1. Data-driven Distributed Observer

To mitigate the impact of actuator faults in MASs, ideally, each agent would access the leader's state directly. However, practical constraints often limit such communication. Thus, it is essential to design observers that enable followers to estimate the leader's state using only local information. In this paper, we propose three distributed observers to estimate the leader's dynamics and state, respectively:

$$\hat{\mathcal{A}}_i(s+1) = \hat{\mathcal{A}}_i(s) + \sigma_i \sum_{j\in\mathcal{N}_i} a_{ij}(\hat{\mathcal{A}}_j(s) - \hat{\mathcal{A}}_i(s)) + \sigma_i\omega_{i0}(\mathcal{A}_0(s) - \hat{\mathcal{A}}_i(s)), \tag{3a}$$

$$\hat{\mathcal{C}}_i(s+1) = \hat{\mathcal{C}}_i(s) + \upsilon_i \sum_{j\in\mathcal{N}_i} a_{ij}(\hat{\mathcal{C}}_j(s) - \hat{\mathcal{C}}_i(s)) + \upsilon_i\omega_{i0}(\mathcal{C}_0(s) - \hat{\mathcal{C}}_i(s)), \tag{3b}$$

$$\zeta_i(s+1) = \hat{\mathcal{A}}_i[\zeta_i(s) + \kappa_i \sum_{j\in\mathcal{N}_i} a_{ij}(\zeta_i(s) - \zeta_j(s)) + \kappa_i\omega_{i0}(\zeta_i(s) - x_0(s))], \tag{3c}$$

where $\hat{\mathcal{A}}_i(s)$, $\hat{\mathcal{C}}_i(s)$ and $\zeta_i(s)$ denote the estimation of the internal dynamics, output dynamics and leader's state, respectively. σ_i, υ_i, and κ_i are the parameters to be designed.

Remark 1. *For the ith agent, the observer relies solely on its own estimate and those of its neighbors to reconstruct the leader's dynamics, without requiring any direct knowledge of the actual leader model. This design reflects the practical reality that precise information about the leader's dynamics is often unavailable in real-world systems. Moreover, since the agents interact only through the exchange of their estimated leader dynamics, rather than their own state information, the proposed approach avoids mutual influence among the agents' states.*

Theorem 1. *Consider the fully heterogeneous nonlinear MASs with the leader's dynamics as* (2)*, let Assumption 1 and Assumption 2 hold and design the distributed observer as* (3)*, then the estimation* $\hat{\mathcal{A}}_i$*,* $\hat{\mathcal{C}}_i$ *and* ζ_i *can converge to the leader's dynamics* $\mathcal{A}_0$*,* $\mathcal{C}_0$ *and the leader's state* x_0 *as* $t \to \infty$ *respectively, if* $0 < \sigma < (2/\rho(\mathcal{H}))$*,* $0 < \upsilon < (2/\rho(\mathcal{H}))$ *and* $0 < \kappa < (2/\rho(\mathcal{H}))$*.*

Proof: Define the estimation errors of the leader's dynamics as

$$\begin{aligned}
\tilde{\mathcal{A}}_i(s+1) =& \hat{\mathcal{A}}_i(s+1) - \mathcal{A}_0 \\
=& \hat{\mathcal{A}}_i(s) + \sigma_i(\sum_{j\in\mathcal{N}_i} a_{ij}(\hat{\mathcal{A}}_j(s) - \hat{\mathcal{A}}_i(s)) + \omega_{i0}(\mathcal{A}_0(s) - \hat{\mathcal{A}}_i(s))) - \mathcal{A}_0 \\
\tilde{\mathcal{C}}_i(s+1) =& \hat{\mathcal{C}}_i(s+1) - \mathcal{C}_0, \\
=& \hat{\mathcal{C}}_i(s) + \upsilon_i \sum_{j\in\mathcal{N}_i} a_{ij}(\hat{\mathcal{C}}_j(s) - \hat{\mathcal{C}}_i(s)) + \upsilon_i\omega_{i0}(C_0(s) - \hat{\mathcal{C}}_i(s)) - \mathcal{C}_0.
\end{aligned}$$

Let $\bar{\tilde{\mathcal{A}}}(s) = [\tilde{\mathcal{A}}_1^{\mathrm{T}}(s), \cdots, \tilde{\mathcal{A}}_{\mathcal{N}}^{\mathrm{T}}(s)]^{\mathrm{T}}$, $\bar{\tilde{\mathcal{C}}}(s) = [\tilde{\mathcal{C}}_1^{\mathrm{T}}(s), \cdots, \tilde{\mathcal{C}}_{\mathcal{N}}^{\mathrm{T}}(s)]^{\mathrm{T}}$, then we have $\bar{\tilde{\mathcal{A}}}(s+1) = (I_{\mathcal{N}} - \sigma(\mathcal{H}\otimes I_{n_0}))\bar{\tilde{\mathcal{A}}}(s)$, $\bar{\tilde{\mathcal{C}}}(s+1) = (I_{\mathcal{N}} - \upsilon(\mathcal{H}\otimes I_{n_0}))\bar{\tilde{\mathcal{C}}}(s)$, where $\mathcal{H} = [h_{ij}]$ with $h_{ii} = \sum_{j\in\mathcal{N}_i} a_{ij} + \omega_{i0}$ and $h_{ij} = -a_{ij}$ for any $i \neq j$, $\sigma = [\sigma_1, \cdots, \sigma_{\mathcal{N}}]^{\mathrm{T}}$ and $\upsilon = [\upsilon_1, \cdots, \upsilon_{\mathcal{N}}]^{\mathrm{T}}$.

Under Assumption 1, all the eigenvalues of $\mathcal{H} = [h_{ij}]$ have real parts. Due to $0 < \sigma_i < (2/\rho(\mathcal{H}))$ and $0 < \upsilon_i < (2/\rho(\mathcal{H}))$, then the martix $(I_{\mathcal{N}} - \sigma_i(\mathcal{H}\otimes I_{n_0}))$ and $(I_{\mathcal{N}} - \upsilon_i(\mathcal{H}\otimes I_{n_0}))$ are Schur. Based on this, we have $\lim_{s\to\infty}\bar{\tilde{\mathcal{A}}}(s) = 0$ and $\lim_{s\to\infty}\bar{\tilde{\mathcal{C}}}(s) = 0$ exponentially.

Combined with the observer (3), the estimation error $\xi_i(s+1) = \zeta_i(s+1) - x_0(s+1)$ can be written as:

$$\begin{aligned}
\xi_i(s+1) =& \mathcal{A}_0\xi_i(s) + \kappa_i\mathcal{A}_0\sum_{j\in\mathcal{N}_i} a_{ij}(\xi_i(s) - \xi_j(s)) + \kappa_i\mathcal{A}_0\omega_{i0}\xi_i(s) + \tilde{\mathcal{A}}_i(s)x_0(s) \\
&+ \tilde{\mathcal{A}}_i(s)\omega_{i0}\xi_i(s) + \kappa_i\tilde{\mathcal{A}}_i(s)\sum_{j\in\mathcal{N}_i} a_{ij}(\xi_i(s) - \xi_j(s))
\end{aligned} \tag{4}$$

Define $\bar{\xi}(s) = [\tilde{\xi}_1^{\mathrm{T}}(s), \cdots, \tilde{\xi}_{\mathcal{N}}^{\mathrm{T}}(s)]^{\mathrm{T}}$, and $\tilde{\mathcal{A}}_m = \mathrm{diag}\{\tilde{\mathcal{A}}_1, \cdots, \tilde{\mathcal{A}}_{\mathcal{N}}\}$, then

$$\begin{aligned}
\bar{\xi}(s+1) =& (I_{\mathcal{N}}\otimes\mathcal{A}_0 - \kappa(\mathcal{H}\otimes\mathcal{A}_0))\bar{\xi}(s) + \tilde{\mathcal{A}}_m(1_{\mathcal{N}}\otimes x_0(s)) \\
&+ \left(\tilde{\mathcal{A}}_m - \kappa\begin{bmatrix} \mathcal{H}_1\otimes\tilde{\mathcal{A}}_1 \\ \vdots \\ \mathcal{H}_{\mathcal{N}}\otimes\tilde{\mathcal{A}}_{\mathcal{N}} \end{bmatrix}\right)\bar{\xi}(s),
\end{aligned} \tag{5}$$

where $\kappa = [\kappa_1, \cdots, \kappa_{\mathcal{N}}]^{\mathrm{T}}$ and $\mathcal{H}_i$ denote the ith row of $\mathcal{H}$.

From Assumption 2 and $\lim_{s\to\infty} \bar{\tilde{\mathcal{A}}}(s) = 0$ exponentially, we have $\tilde{\mathcal{A}}_m(1_{\mathcal{N}} \otimes x_0(s))$ will decay to zero exponentially.

In order to reduce the complexity of subsequent derivation, define

$$\mathcal{F}_1 = I_{\mathcal{N}} \otimes \mathcal{A}_0 - \kappa(\mathcal{H} \otimes \mathcal{A}_0), \quad \mathcal{F}_2 = \left(\tilde{\mathcal{A}}_m - \kappa \begin{bmatrix} \mathcal{H}_1 \otimes \tilde{\mathcal{A}}_1 \\ \vdots \\ \mathcal{H}_{\mathcal{N}} \otimes \tilde{\mathcal{A}}_{\mathcal{N}} \end{bmatrix} \right)$$

The eigenvalues of $\mathcal{F}_1$ can be expressed as $\lambda(\mathcal{F}_1) = \lambda(\mathcal{A}_0)(1 - \kappa\lambda(\mathcal{H}))$. For $0 < \kappa < \frac{2}{\rho(\mathcal{H})}$, we have$|1 - \kappa\lambda_i(\mathcal{H})| < 1, \quad \forall i$. Combined with $|\lambda(\mathcal{A}_0)| \leq 1$, we can obtain $|\lambda(\mathcal{F}_1)| = |\lambda(\mathcal{A}_0)||(1 - \kappa\lambda(\mathcal{H}))| < 1, \quad \forall i, j$. Then, $\mathcal{F}_1$ is Schur. Therefore, there exist a symmetric positive definite matrix $\mathcal{P}$ such that $\mathcal{F}_1^{\mathrm{T}}\mathcal{P}\mathcal{F}_1 - \mathcal{P} = -\mathcal{Q}$, for any symmetric positive definite matrix $\mathcal{Q}$.

Select Lyapunuv function as $\mathcal{L}(s) = \bar{\xi}^{\mathrm{T}}(s)\mathcal{P}\bar{\xi}(s)$, and then we have

$$\begin{aligned} \Delta\mathcal{L}(s+1) &= \mathcal{L}(s+1) - \mathcal{L}(s) \\ &= (\mathcal{F}_1\bar{\xi}(s) + \mathcal{F}_2\bar{\xi}(s))^{\mathrm{T}}\mathcal{P}(\mathcal{F}_1\bar{\xi}(s) + \mathcal{F}_2\bar{\xi}(s)) - \bar{\xi}^{\mathrm{T}}(s)\mathcal{P}\bar{\xi}(s) \\ &= -\bar{\xi}^{\mathrm{T}}(s)(\mathcal{Q} - 2\mathcal{F}_1^{\mathrm{T}}\mathcal{P}\mathcal{F}_2 - \mathcal{F}_2^{\mathrm{T}}\mathcal{P}\mathcal{F}_2)\bar{\xi}(s), \end{aligned} \tag{6}$$

Since $\tilde{\mathcal{A}}i$ converges exponentially and all variables are bounded, we have $\lim_{s\to\infty} \mathcal{F}_2 = 0$. Thus, there exist $S \in \mathbb{Z}^+$ and $\gamma > 0$ such that for all $s \geq S$, $\Delta\mathcal{L}(s) < -\gamma|\bar{\xi}(s)|^2$.

This implies that the error dynamics described by equation (5) are exponentially stable, and hence the state estimation error $\bar{\xi}(s)$ is uniformly bounded and converges to zero exponentially. Furthermore, since $\mathcal{F}_1$ is a Schur matrix, there exists a class $\mathcal{K}$ function $\Phi(\cdot)$ such that the solution satisfies the bound $\limsup_{s\to\infty} \|\xi(s)\| \leq \Phi(\limsup_{s\to\infty} \|\mathcal{F}_1\bar{\xi}(s) + \mathcal{F}_2\bar{\xi}(s) + \tilde{\mathcal{A}}_m(1_{\mathcal{N}} \otimes x_0(s))\|)$.

Since $\xi(s)$ is bounded, $\mathcal{F}_1$ and $\mathcal{F}_2$ tend to zero, then $\xi(s)$ converges to zero exponentially. ■

3.2. Data-driven Security Controller

Before designing the data-driven security controller, dynamic linearization is employed to generate an online data model for the ith follower under actuator faults and output saturation.

Assumption 3. *For the ith follower in the MAS, the generalized Lipschitz condition should be satisfied, which can be shown as follows*

$$\|\Delta y_i(s+1)\| \leq \varpi_i |u_{ri}(s+1) - u_{ri}(s)|, \quad |u_{ri}(s+1) - u_{ri}(s)| \neq 0$$

where $\Delta y_i(s+1) = y_i(s+1) - y_i(s)$, $u_{ri}(s) = u_i(s) + u_{fi}(s)$, $\varpi_i > 0$ is a constant.

Lemma 1. *[20] Under Assumption 3 and $|u_{ri}(s+1) - u_{ri}(s)| \neq 0$, the ith follower's dynamics with actuator faults can be reformulated as a data model:*

$$\Delta y_i(s+1) = \varphi_i(s)\Delta u_i(s) + \varphi_i(s)\Delta u_{fi}(s) \tag{7}$$

where $\varphi_i(s)$ is the pseudo-partial-derivative(PPD), $\Delta u_i(s) = u_i(s) - u_i(s-1)$,$\Delta u_{fi}(s) = u_{fi}(s) - u_{fi}(s-1)$, $|\Delta u_{fi}(s)| < u_{fm}$,$|\varphi_i(s)| \leq c$.

Consider the sensor saturation of the ith follower, we have

$$\hat{y}_i(s) = sat_{\bar{y}_i}(y_i(s)) = \begin{cases} \bar{y}_i, & y_i(s) > \bar{y}_i \\ y_i(s), & -\bar{y}_i \leq y_i(s) \leq \bar{y}_i \\ -\bar{y}_i, & y_i(s) < -\bar{y}_i \end{cases} \tag{8}$$

where $\bar{y}_i$ denotes the unknown boundary of sensor measurement.

Then, the data model of the ith follower with actuator faults and sensor saturation can be written as

$$\Delta\hat{y}(s+1) = \psi_i(s)(\Delta u_i(s) + \Delta u_{fi}(s)) \tag{9}$$

where $\psi_i(s)$ denotes the PPD of the ith follower with actuator faults and sensor saturation.

Select the cost function $\mathcal{J}_i(u_i(s))$ of the ith follower as

$$\mathcal{J}_i(u_i(s)) = \left|\hat{\zeta}_i(s+1) - \hat{y}_i(s+1)\right|^2 + \alpha_i |\Delta u_i(s)|^2 \tag{10}$$

where α_i is the weighting parameter to limit the change of the input of the ith follower, $\hat{\zeta}_i(s+1) = \hat{\mathcal{C}}_i(s+1)\zeta_i(s+1)$.

Substituting (3c) and (9) into (10), and then minimizing (10) with respect to $\Delta u_i(s)$, we can obtain

$$\Delta u_i(s) = \psi_i(s)\frac{\varsigma_i(\hat{\zeta}_i(s+1) - \hat{y}_i(s)) - \eta_i\psi_i(s)\Delta\hat{u}_{fi}(s)}{\alpha_i + \psi_i^2(s)} \tag{11}$$

where $\Delta\hat{u}_{fi}(s)$ is the estimation of $\Delta u_{fi}(s)$, $\varsigma_i \in (0,1]$ and $\eta_i \in (0,1]$ are step factors for flexibility.

Consider the cost function $\mathcal{J}_i(\psi_i)$ with respect to ψ_i as

$$\mathcal{J}_i(\psi_i) = |\Delta y_i(s) - \psi_i(s)\Delta u_{ri}(s-1)|^2 + \lambda_i|\psi_i(s) - \hat{\psi}_i(s-1)|^2 \tag{12}$$

where λ_i is a positive weighting parameter.

Then, the PPD estimate $\hat{\psi}_i(s)$ is obtained by minimizing (12), so that

$$\hat{\psi}_i(s) = \hat{\psi}_i(s-1) + \frac{\rho_i\Delta u_{ri}(s-1)}{\lambda_i+\Delta u_{ri}^2(s-1)}[\Delta y_i(s) - \hat{\psi}_i(s-1)\Delta u_{ri}(s-1)] \tag{13}$$

where $\rho_i \in (0,1]$ is the step size.

Combining (11) and (13), the model-free adaptive security controller for the ith follower is shown as

$$\hat{\psi}_i(s) = \hat{\psi}_i(s-1) + \frac{\rho_i\Delta u_{ri}(s-1)}{\lambda_i+\Delta u_{ri}^2(s-1)}[\Delta y_i(s) - \hat{\psi}_i(s-1)\Delta u_{ri}(s-1)] \tag{14a}$$

$$\hat{\psi}_i(s) = \hat{\psi}_i(1), if \quad \text{sign}(\hat{\psi}_i(s)) \neq \text{sign}(\hat{\psi}_i(1)) or |\hat{\psi}_i(s)| < \epsilon \tag{14b}$$

$$\Delta u_i(s) = \hat{\psi}_i(s)\frac{\varsigma_i(\hat{\zeta}_i(s+1)-\hat{y}_i(s))-\eta_i\hat{\psi}_i(s)\Delta\hat{u}_{fi}(s)}{\alpha_i+\hat{\psi}_i^2(s)} \tag{14c}$$

where

$$\Delta\hat{u}_{fi}(s) = \frac{\hat{\psi}_i^2(s)\Delta\hat{u}_{fi}(s-1)}{\alpha_i+\hat{\psi}_i^2(s)} - \frac{m_i(\hat{\zeta}_i(s)-\hat{y}_i(s))}{\hat{\psi}_i(s)} \tag{15}$$

and m_i is a constant, $\hat{\psi}_i(1)$ is the initial value of $\hat{\psi}_i(s)$, ϵ is a positive constant.

Remark 2. *With the introduction of the hierarchical control framework, the entire MAS is effectively decoupled. Consequently, the consensus control problem is transformed into a set of independent tracking control problems for individual agents. This transformation significantly reduces the coupling of control parameters among agents, thereby simplifying the parameter tuning process. Moreover, since the design no longer relies on consensus error terms, the control error of a single agent does not propagate to others, thus preserving the overall system performance. This decoupled structure enhances both the robustness and scalability of the control strategy, making it well-suited for large-scale and dynamically evolving MASs.*

3.3. Algorithm Analysis

In this subsection, we analyze the proposed algorithm from three key practical perspectives: computational complexity, communication requirements, and parameter tuning guidelines.

3.3.1. Computational Complexity

The proposed control framework consists of two main components: the distributed data-driven observer and the model-free adaptive controller.

The observer module consists of three distributed recursive updates of $\hat{\mathcal{A}}_0$ and $\hat{\mathcal{C}}_0$ involve $\mathcal{O}(d|\mathcal{N}_i|)$ operations due to local averaging, where d is the dimension of system states and $|\mathcal{N}_i|$ is the size of the ith agent's neighborhood. The update of the state estimator $\zeta_i(s)$ further requires an additional matrix-vector multiplication, leading to a total per-agent complexity of $\mathcal{O}(d^2 + d|\mathcal{N}_i|)$. Consequently, the system-wide complexity of the estimation layer is $\mathcal{O}(d^2\mathcal{N} + d|E|)$, where $\mathcal{N}$ denotes the number of agents and $|E| = \sum_{i=1}^{\mathcal{N}} \mathcal{N}_i$ denotes the number of communication links in the network.

The adaptive control module includes a scalar parameter update law, a conditional reset mechanism, and a distributed control law involving vector operations. The parameter update and reset check involve $\mathcal{O}(1)$ scalar operations per agent. The control law involves a vector subtraction and scalar weighting, leading to $\mathcal{O}(d)$ complexity per agent. Therefore, the overall control module incurs: $\mathcal{O}(d\mathcal{N})$ operations per step.

Hence, combining both modules, the total system-wide computational complexity per time step is given by: $\mathcal{O}(d^2\mathcal{N} + d|E|)$. For the Assumption 1, the complexity simplifies to $\mathcal{O}(d^2\mathcal{N})$. This ensures good scalability for large-scale MASs under the proposed scheme.

3.3.2. Computational Complexity

Since the framework is designed based on a fully distributed architecture, it yields two key advantages. First, each agent exchanges information solely with its immediate neighbors, as defined by the communication topology. Second, the amount of data exchanged at each time step remains fixed and does not scale with the size of the overall system. These properties make the framework highly suitable for practical deployment, where communication can be efficiently handled over low-bandwidth local wireless networks.

3.3.3. Parameter Tuning Guidelines

In the proposed data-driven hierarchical security control algorithm (14), several parameters, including α_i, λ_i, ρ_i, η_i, and ς_i, require careful tuning to achieve satisfactory control performance. The regularization factor α_i balances responsiveness and input smoothness: smaller values yield faster response but risk instability; larger values enhance robustness. Parameters

λ_i and ρ_i govern the PPD estimation trade-off between accuracy, smoothness, and adaptation speed. A smaller λ_i or larger ρ_i improves response but increases disturbance sensitivity. The step sizes ς_i and η_i control tracking strength and fault compensation. Higher ς_i improves tracking, while η_i balances fault rejection and stability. Lastly, m_i adjusts the fault estimator's update rate, with moderate values ensuring stable fault detection.

4. Stability Analysis

Before the stability analysis of MASs with actuator faults and sensor saturation, the following assumption is commonly adopted.

Assumption 4. *[9]* $\phi_i(s)>\phi_s>0$, $\forall s\in\mathbb{N}^+$, *where* ϕ_s *is a positive constant.*

Lemma 2. *[20] Define the tracking error and the measurement error of the* i*th follower with sensor saturation in the MASs as* $e_{si}(s)=y_0(s)-y_i(s)$ *and* $\check{e}_{si}(s)=y_0(s)-\hat{y}_i(s)$*, we have* $\check{e}_{si}(s)=\hbar_i(s)e_{si}(s)$*, where*

$$\hbar_i(s)=\begin{cases}\frac{y_0(s)+\bar{y}_i}{e_{si}(s)}, & e_{si}(s)>y_0(s)+\bar{y}_i\\ 1, & y_0(s)-\bar{y}_i\le e_{si}(s)\le y_0(s)+\bar{y}_i\\ \frac{y_0(s)-\bar{y}_i}{e_{si}(s)}, & e_{si}(s)<y_0(s)-\bar{y}_i\end{cases}$$

Theorem 2. *Consider the MASs with actuator faults as* (1)*, let Assumption 1 hold and design the controller as* (14)*, the tracking error of the MASs will be bounded if the following inequalities are satisfied*

$$\begin{aligned}&3p\|(I-\aleph\Psi(s)\Lambda(s))\|^2>-3q\|(I-\aleph\Psi(s)\Lambda(s))\|^2-p\\&3p\varkappa^2\|\Psi(s)\|^2\|\Xi(s)\|^2>(1-3\|[\Xi(s+1)-\beth\Psi^{-1}(s+1)\varkappa\Psi(s)\Xi(s)]\|^2)q\end{aligned}\quad(16)$$

Proof: This proof is divided into two parts, proving the boundedness of the estimation of PPD and the tracking error, respectively.

Part 1: This part consists of two cases. In case 1, the function (14b) is satisfied, and it is obvious that the estimation of PPD is bounded.

In case 2, substituting (14a) into the estimation error $e_{\psi i}(s)=\hat{\psi}_i(s)-\psi_i(s)$ yields:

$$\begin{aligned}e_{\psi i}(s)&=e_{\psi i}(s-1)+\psi_i(s-1)-\psi_i(s)+\tfrac{\rho_i\Delta u_{ri}(s-1)}{\lambda_i+\Delta u_{ri}^2(s-1)}[\Delta y_i(s)-\hat{\psi}_i(s-1)\Delta u_{ri}(s-1)]\\&=\psi_i(s-1)+(1-\tfrac{\rho_i\Delta u_{ri}(s-1)}{\lambda_i+\Delta u_{ri}^2(s-z1)})e_{\psi i}(s-1)-\psi_i(s)+\psi_i(s-1)\Delta u_{fi}(s-1)\tfrac{\rho_i\Delta u_{ri}(s-1)}{\lambda_i+\Delta u_{ri}^2(s-1)}\end{aligned}\quad(17)$$

Then, we can obtain

$$\begin{aligned}|e_{\psi i}(s)| \leq & |\psi_i(s)-\psi_i(s-1)|+|\psi_i(s-1)\Delta u_{fi}(s-1)\tfrac{\rho_i \Delta u_{ri}(s-1)}{\lambda_i+\Delta u_{ri}^2(s-1)}| \\ & +|1-\tfrac{\rho_i \Delta u_{ri}(s-1)}{\lambda_i+\Delta u_{ri}^2(s-1)}||\tau_i(s-1)| \end{aligned} \tag{18}$$

Also, it is easy to gain $|\frac{\rho_i \Delta u_{ri}(s-1)}{\lambda_i+\Delta u_{ri}^2(s-1)}| \leq \frac{\rho_i|\Delta u_{ri}(s-1)|}{2\sqrt{\lambda_i}|\Delta u_{ri}(s-1)|} = \frac{\rho_i}{2\sqrt{\lambda_i}}$, $|\psi_i(s)-\psi_i(s-1)| \leq 2\varpi_i$ and $|\psi_i(s)| \leq \varpi_i$. Thus, we can obtain

$$\begin{aligned}|e_{\psi i}(s)| \leq & \Upsilon_i|e_{\psi i}(s-1)|+2\varpi_i+\tfrac{\varpi_i u_{fm}\rho_i}{2\sqrt{\lambda_i}} \\ \leq & \Upsilon_i^2|e_{\psi i}(s-1)|+\Upsilon_i(2\varpi_i+\tfrac{\varpi_i u_{fm}\rho_i}{2\sqrt{\lambda_i}})+2\varpi_i+\tfrac{\varpi_i u_{fm}\rho_i}{2\sqrt{\lambda_i}} \\ & \cdots \\ \leq & \Upsilon_i^{k-1}|e_{\psi i}(1)|+\tfrac{2\varpi_i+\frac{\varpi_i u_{fm}\rho_i}{2\sqrt{\lambda_i}}}{1-\Upsilon_i} \end{aligned} \tag{19}$$

where Υ_i is a positive constant that be obtained by selecting ρ_i and λ_i to satisfy $0<|1-\frac{\rho_i \Delta u_{ri}(s-1)}{\lambda_i+\Delta u_{ri}^2(s-1)}| \leq \Upsilon_i < 1$.

Based on the above analysis, since both $e_{\psi i}(s)$ and $\psi_i(s)$ are bounded, it follows that $\hat{\psi}_i(s)$ is also bounded.

Part 2: In this part, we will give the proof of the boundedness of the tracking error $e_{Si}(s)$. By Theorem 1 and Lemma 2, if $\hat{e}_{Si}(s)=\hat{\zeta}_i(s)-\hat{y}_i(s)$ remains bounded as $s\to\infty$, then $e_{Si}(s)$ is also bounded.

From function (14c), we have

$$\mathbf{U}(s)=\mathbf{U}(s-1)+\aleph\Lambda(s)\mathbf{e}_S(s)-\varkappa\Xi(s)\Delta\hat{\mathbf{U}}_f(s) \tag{20}$$

where $\aleph=\mathrm{diag}\{\sigma_1,\sigma_2,\cdots,\sigma_{\mathcal{N}}\}$, $\varkappa=\mathrm{diag}\{\eta_1,\eta_2,\cdots,\eta_{\mathcal{N}}\}$, $\mathbf{U}(s)=[u_1(s),$ $u_2(s),\cdots,u_{\mathcal{N}}(s)]^{\mathrm{T}}$, $\Lambda(s)=\mathrm{diag}\{\frac{\hat{\psi}_1(s)}{\alpha_1+\hat{\psi}_1^2(s)},\frac{\hat{\psi}_2(s)}{\alpha_2+\hat{\psi}_2^2(s)},\cdots,\frac{\hat{\psi}_{\mathcal{N}(s)}}{\alpha_{\mathcal{N}}+\hat{\psi}_{\mathcal{N}}^2(s)}\}$,$\mathbf{e}_S(s)=$ $[\hat{e}_{S1}(s),\hat{e}_{S2}(s),\cdots,\hat{e}_{S\mathcal{N}}(s)]^{\mathrm{T}}$, $\Delta\hat{\mathbf{U}}_f(s)=[\Delta\hat{u}_{f1}(s),\Delta\hat{u}_{f2}(s),\cdots,\Delta\hat{u}_{f\mathcal{N}}(s)]^{\mathrm{T}}$, and $\Xi(s)=\mathrm{diag}\{\frac{\hat{\psi}_1^2(s)}{\alpha_1+\hat{\psi}_1^2(s)},\frac{\hat{\psi}_2^2(s)}{\alpha_2+\hat{\psi}_2^2(s)},\cdots,\frac{\hat{\psi}_{\mathcal{N}(s)}^2}{\alpha_{\mathcal{N}}+\hat{\psi}_{\mathcal{N}}^2(s)}\}$.

Substituting (20) into (9), we can obtain

$$\mathbf{y}(s+1)=\mathbf{y}(s)+\Psi(s)(\aleph\Lambda(s)\mathbf{e}_S(s)+\Delta\mathbf{U}_{fi}(s)-\varkappa\Xi(s)\Delta\hat{\mathbf{U}}_f(s)) \tag{21}$$

where $\Delta\mathbf{U}_f(s)=[\Delta u_{f1}(s),\Delta u_{f2}(s),\cdots,\Delta u_{f\mathcal{N}}(s)]^{\mathrm{T}}$ and $\Psi(s)=\mathrm{diag}\{\hat{\psi}_1(s),$ $\hat{\psi}_2(s),\cdots,\hat{\psi_{\mathcal{N}}}(s)\}$.

Then, we can obtain

$$\begin{aligned}\mathbf{e}_S(s+1) &= \mathbf{e}_S(s) - \aleph\Psi(s)\Lambda(s)\mathbf{e}_S(s) - \Psi(s)\Delta\mathbf{U}_f(s) + \varkappa\Psi(s)\Xi(s)\Delta\hat{\mathbf{U}}_f(s) + \bar{\hat{\zeta}}(s+1) - \bar{\hat{\zeta}}(s) \\ &= (I - \aleph\Psi(s)\Lambda(s))\mathbf{e}_S(s) + (\varkappa\Psi(s)\Xi(s) - \Psi(s))\Delta\mathbf{U}_f(s) + \Delta\bar{\hat{\zeta}}(s+1) + \varkappa\Psi(s)\Xi(s)\Delta\tilde{\mathbf{U}}_f(s) \quad (22)\end{aligned}$$

where $\bar{\hat{\zeta}}(s) = [\hat{\zeta}_1(s), \hat{\zeta}_2(s), \cdots, \hat{\zeta}_{\mathcal{N}}(s)]^{\mathrm{T}}$.

According to function (15), we have

$$\Delta\hat{\mathbf{U}}_f(s+1) = \Xi(s+1)\Delta\hat{\mathbf{U}}_f(s) - \beth\Psi^{-1}(s+1)\mathbf{e}_S(s+1) \quad (23)$$

Then, we can obtain

$$\begin{aligned}\Delta\tilde{\mathbf{U}}_f(s+1) &= \Delta\hat{\mathbf{U}}_f(s+1) - \Delta\mathbf{U}_f(s+1) \\ &= \Xi(s+1)\Delta\hat{\mathbf{U}}_f(s) - \beth\Psi^{-1}(s+1)\mathbf{e}_S(s+1) - \Delta\mathbf{U}_f(s+1) \\ &= \Xi(s+1)\Delta\tilde{\mathbf{U}}_f(s) + \Xi(s+1)\Delta\mathbf{U}_f(s) - \Delta\mathbf{U}_f(s+1) - \beth\Psi^{-1}(s+1)\mathbf{e}_S(s+1) \quad (24)\end{aligned}$$

Substituting (22) into (24), we can obtain

$$\begin{aligned}\Delta\tilde{\mathbf{U}}_f(s+1) &= [\Xi(s+1) - \beth\Psi^{-1}(s+1)\varkappa\Psi(s)\Xi(s)]\Delta\tilde{\mathbf{U}}_f(s) + [\Xi(s+1) - \beth\Psi^{-1}(s+1)(\varkappa \\ &\times \Psi(s)\Xi(s) - \Psi(s))]\Delta\mathbf{U}_f(s) - \beth\Psi^{-1}(s+1)(I - \aleph\Psi(s)\Lambda(s))\mathbf{e}_S(s) - \Delta\mathbf{U}_f(s+1) - \beth \\ &\times \Psi^{-1}(s+1)\Delta\bar{\hat{\zeta}}(s+1) \quad (25)\end{aligned}$$

Select the Lyapunov function as $\mathcal{L}_S(s) = p\mathbf{e}_S^{\mathrm{T}}(s)\mathbf{e}_S + q\Delta\tilde{\mathbf{U}}_f^{\mathrm{T}}(s)\Delta\tilde{\mathbf{U}}_f(s)$, where $p > 0, q > 0$.

Then, the difference of $\mathcal{L}$ can be obtained as

$$\begin{aligned}\Delta\mathcal{L}_S(s+1) =& p\mathbf{e}_S^{\mathrm{T}}(s+1)\mathbf{e}_S(s+1) + q\Delta\tilde{\mathbf{U}}_f^{\mathrm{T}}(s+1)\Delta\tilde{\mathbf{U}}_f(s+1) \\ &- p\mathbf{e}_S^{\mathrm{T}}(s)\mathbf{e}_S(s) - q\Delta\tilde{\mathbf{U}}_f^{\mathrm{T}}(s)\Delta\tilde{\mathbf{U}}_f(s) \quad (26)\end{aligned}$$

Substituting (22) and (25) into (26), we have

$$\begin{aligned}&\Delta\mathcal{L}_S(s+1) \\ &= [(I - \aleph\Psi(s)\Lambda(s))\mathbf{e}_S(s) + \varkappa\Psi(s)\Xi(s)\Delta\tilde{\mathbf{U}}_f(s) + (\varkappa\Psi(s)\Xi(s) - \Psi(s))\Delta\mathbf{U}_f(s) + \Delta\bar{\hat{\zeta}}(s+1)]^{\mathrm{T}} \\ &\times [(I - \aleph\Psi(s)\Lambda(s))\mathbf{e}_S(s) + \varkappa\Psi(s)\Xi(s)\Delta\tilde{\mathbf{U}}_f(s) + \varkappa\Psi(s)\Xi(s)\Delta\mathbf{U}_f(s) - \Psi(s)\Delta\mathbf{U}_f(s) \\ &+ \Delta\bar{\hat{\zeta}}(s+1)] + q\{[\Xi(s+1) - \beth\Psi^{-1}(s+1)\varkappa\Psi(s)\Xi(s)]\Delta\tilde{\mathbf{U}}_f(s) + [\Xi(s+1) - \beth\Psi^{-1}(s+1) \\ &\times (\varkappa\Psi(s)\Xi(s) - \Psi(s))]\Delta\mathbf{U}_f(s) - \beth\Psi^{-1}(s+1)(I - \aleph\Psi(s)\Lambda(s))\mathbf{e}_S(s) - \Delta\mathbf{U}_f(s+1) - \beth \\ &\times \Psi^{-1}(s+1)\Delta\bar{\hat{\zeta}}(s+1)\}^{\mathrm{T}}\{[\Xi(s+1) - \beth\Psi^{-1}(s+1)\varkappa\Psi(s)\Xi(s)]\Delta\tilde{\mathbf{U}}_f(s) + [\Xi(s+1) - \beth \\ &\times \Psi^{-1}(s+1)(\varkappa\Psi(s)\Xi(s) - \Psi(s))]\Delta\mathbf{U}_f(s) - \beth\Psi^{-1}(s+1)(I - \aleph\Psi(s)\Lambda(s))\mathbf{e}_S(s) \\ &- \Delta\mathbf{U}_f(s+1) - \beth\Psi^{-1}(s+1)\Delta\bar{\hat{\zeta}}(s+1)\} - p\mathbf{e}_S^{\mathrm{T}}(s)\mathbf{e}_S(s) - q\Delta\tilde{\mathbf{U}}_f^{\mathrm{T}}(s)\Delta\tilde{\mathbf{U}}_f(s) \quad (27)\end{aligned}$$

For the boundedness of $\bar{\hat{\zeta}}(s)$, $\Delta\mathbf{U}_f(s)$, $\Psi(s)$ and $\hat{\Psi}(s)$, it is possible to be obtain that $\|(\varkappa\Psi(s)\Xi(s)-\Psi(s))\Delta\mathbf{U}_f(s)+\Delta\bar{\hat{\zeta}}\| \leq \mathbf{M}_1$, $\|[\Xi(s+1)-\daleth\Psi^{-1}(s+1)(\varkappa\Psi(s)\Xi(s)-\Psi(s))]\Delta\mathbf{U}_f(s)-\Delta\mathbf{U}_f(s+1)-\daleth\Psi^{-1}(s+1)\Delta\bar{\hat{\zeta}}(s+1)\| \leq \mathbf{M}_2$, and $\Psi_l(s) \leq \|\hat{\Psi}(s)\| \leq \Psi_u(s)$. Then we have

$$
\begin{aligned}
&\Delta\mathcal{L}_S(s+1)\\
&\leq 3p(\|(I-\aleph\Psi(s)\Lambda(s))\|^2\|\mathbf{e}_S(s)\|^2+\mathbf{M}_1^2+\varkappa^2\|\Psi(s)\|^2\|\Xi(s)\|^2\|\Delta\tilde{\mathbf{U}}_f(s)\|^2)\\
&+3q(\|[\Xi(s+1)-\daleth\Psi^{-1}(s+1)\times\varkappa\Psi(s)\Xi(s)]\|^2\|\Delta\tilde{\mathbf{U}}_f(s)\|^2+\mathbf{M}_2^2+\|\daleth\|^2\\
&\times\|\Psi^{-1}(s+1)\|^2\|(I-\aleph\Psi(s)\Lambda(s))\|^2\|\mathbf{e}_S(s)\|^2)-p\|\mathbf{e}_S(s)\|^2-q\|\Delta\tilde{\mathbf{U}}_f\|^2\\
&\leq(3p\|(I-\aleph\Psi(s)\Lambda(s))\|^2+3q\|(I-\aleph\Psi(s)\Lambda(s))\|^2-p)\|\mathbf{e}_S(s)\|^2\\
&+(3p\varkappa^2\|\Psi(s)\|^2\|\Xi(s)\|^2+3q\|[\Xi(s+1)-\daleth\Psi^{-1}(s+1)\varkappa\Psi(s)\Xi(s)]\|^2\\
&-q)\|\Delta\tilde{\mathbf{U}}_f(s)\|^2+3p\mathbf{M}_1^2+3q\mathbf{M}_2^2\\
&\leq \mathit{\Pi}_1\|\mathbf{e}_S(s)\|^2+\mathit{\Pi}_2\|\Delta\tilde{\mathbf{U}}_f(s)\|^2+\mathit{\Pi}_3
\end{aligned}
\tag{28}
$$

where $\mathit{\Pi}_1=3p\|(I-\aleph\Psi(s)\Lambda(s))\|^2+3q\|(I-\aleph\Psi(s)\Lambda(s))\|^2-p$, $\mathit{\Pi}_2=3p\varkappa^2\|\Psi(s)\|^2\|\Xi(s)\|^2-q+3q\|[\Xi(s+1)-\daleth\Psi^{-1}(s+1)\varkappa\Psi(s)\Xi(s)]\|^2$ and $\mathit{\Pi}_3=3p\mathbf{M}_1^2+3q\mathbf{M}_2^2$.

From the (16), $\mathit{\Pi}_1$ and $\mathit{\Pi}_2$ are all positive constant. Based on the Lyapunov stability theory, we can obtain $\Delta\mathcal{L}_S(s+1) \leq 0$ if at least one of the following inequalities holds $\|\mathbf{e}_S(s)\| > \sqrt{\frac{\mathit{\Pi}_3}{\mathit{\Pi}_1}}$, $\|\Delta\tilde{\mathbf{U}}_f(s)\| > \sqrt{\frac{\mathit{\Pi}_3}{\mathit{\Pi}_1}}$. Therefore, $\mathbf{e}_S(s)$ and $\Delta\tilde{\mathbf{U}}_f(s)$ are bounded. ■

5. Simulation Examples

5.1. Numerical Simulation 1

Consider a heterogeneous MAS with one leader and three followers, where the leader's state converges to zero. The communication topology is depicted in Figure 1, and the follower dynamics are given as follows:

$$y_1(s+1) = 0.2u_1(s) + \frac{y_1(s)u_1^2(s)}{1+y_1^2(s)} \tag{29}$$

$$y_2(s+1) = 0.5u_2(s) + \frac{y_2(s)u_2(s)}{1+y_2^3(s)} \tag{30}$$

$$y_3(s+1) = u_3(s) + \sin(y_3(s)) \tag{31}$$

Denote the dynamics of the leader as:

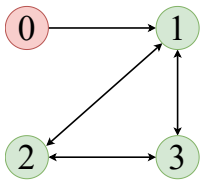

Figure 1: The communication graph of the numerical simulation 1

$$x_0(k+1) = \begin{bmatrix} 0.5 & 0.5 \\ -0.9 & 1 \end{bmatrix} x_0(k), \quad y_0(k) = \begin{bmatrix} 0 & 1 \end{bmatrix} x_0(k). \tag{32}$$

Moreover, assume the actuator faults occur on follower 1 as $\Delta u_{f1} = 0.05\sin(0.5s\pi/150)$.

The observer parameters are set as $\sigma_i = 0.3$, $\upsilon_i = 0.3$, $\kappa_i = 0.4$ $(i = 1, 2, 3)$. The adaptive controller parameters are: $m_1 = 0.4$, $\varsigma_1 = 0.7$, $\varsigma_2 = 0.99$, $\varsigma_3 = 0.9$, $\alpha_1 = 0.1$, $\alpha_2 = 0.05$, $\alpha_3 = 1$, $\rho_1 = 0.1$, $\rho_2 = 0.3$, $\rho_3 = 0.13$, $\lambda_1 = 0.95$, $\lambda_2 = 0.1$, $\lambda_3 = 0.9$. The sensor measurement bound is $\bar{y}_i = 0.3$ for $i = 1, 2, 3$. Initial states are set as $x_0 = [1, 1]^{\mathrm{T}}$ and $y_1 = y_2 = y_3 = 0$.

The followers' observation errors with respect to the leader's dynamics and output are shown in Figure 2 and Figure 3, respectively. As illustrated in Figure 2, the distributed observer accurately estimates the leader's dynamics by the 40th step. Similarly, Figure 3 shows that the leader's output is effectively estimated by the designed observer for the followers after the 120th step. These results validate the effectiveness of the proposed distributed observer in enabling accurate state and output estimation, which is essential for achieving reliable consensus tracking in heterogeneous MASs.

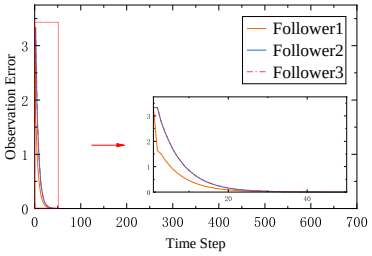

(a) $\|e_{\mathcal{A}i}\|^2 = \|\hat{\mathcal{A}}_i - \mathcal{A}_0\|^2$

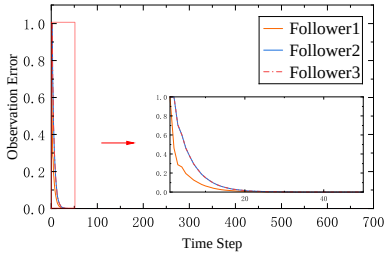

(b) $\|e_{\mathcal{C}i}\|^2 = \|\hat{\mathcal{C}}_i - \mathcal{C}_0\|^2$

Figure 2: Observation errors of the followers relative to the dynamics of the leader.

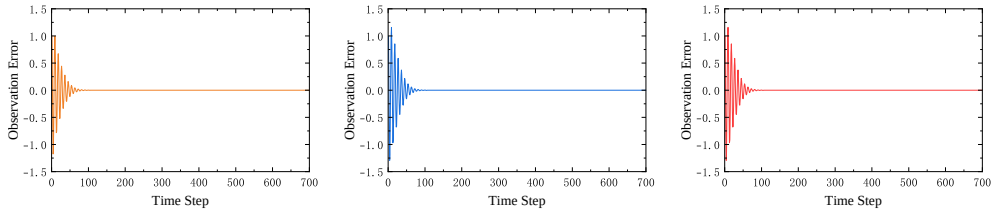

(a) (b) (c)

Figure 3: The followers' observation errors relative to the leader's output. (a)Follower 1 (b)Follower 2 (c)Follower 3

Based on the effectiveness of the distributed observers, the tracking performance of the followers and the behavior of the adaptive actuator fault estimator are illustrated in Figure 4. As shown in Figures 4(a), 4(b), and 4(c), the followers successfully track the leader's output after the 200th step, despite the presence of actuator faults. Additionally, Figure 4(d) demonstrates that the adaptive fault estimator accurately identifies the actuator fault increments after the 250th step, with fast convergence and minimal estimation error, contributing to the overall robustness of the control system.

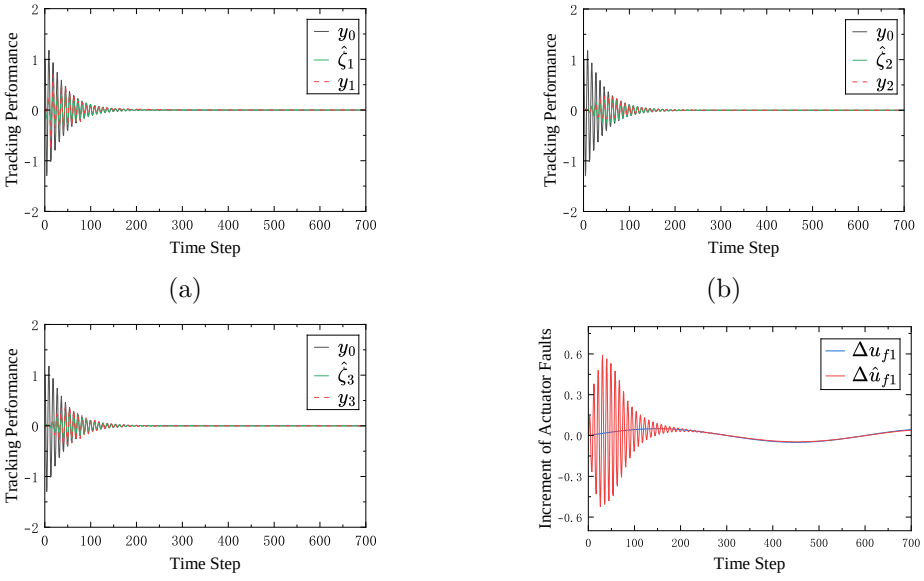

(a) (b) (c) (d)

Figure 4: Performance of followers and adaptive actuator estimator under the proposed control algorithm. (a),(b) and (c) are the tracking performances of Follower 1, Follower 2, and Follower 3, respectively. (d) is the performance of the adaptive actuator estimator.

Furthermore, Figures 5(a), 5(b), and 5(c) show the tracking performance of the followers when the adaptive actuator estimator operates under different parameter configurations. A comparison between Figures 4 and 5 reveals that variations in the adaptive fault estimator's performance affect only the faulty agent, while the tracking behavior of the other agents remains unaffected. This highlights a key advantage of the proposed hierarchical control algorithm: fault isolation. By localizing fault effects, the system maintains stability and consensus tracking despite estimator perturbations, confirming the robustness, scalability, and fault tolerance of the distributed data-driven approach in heterogeneous MASs.

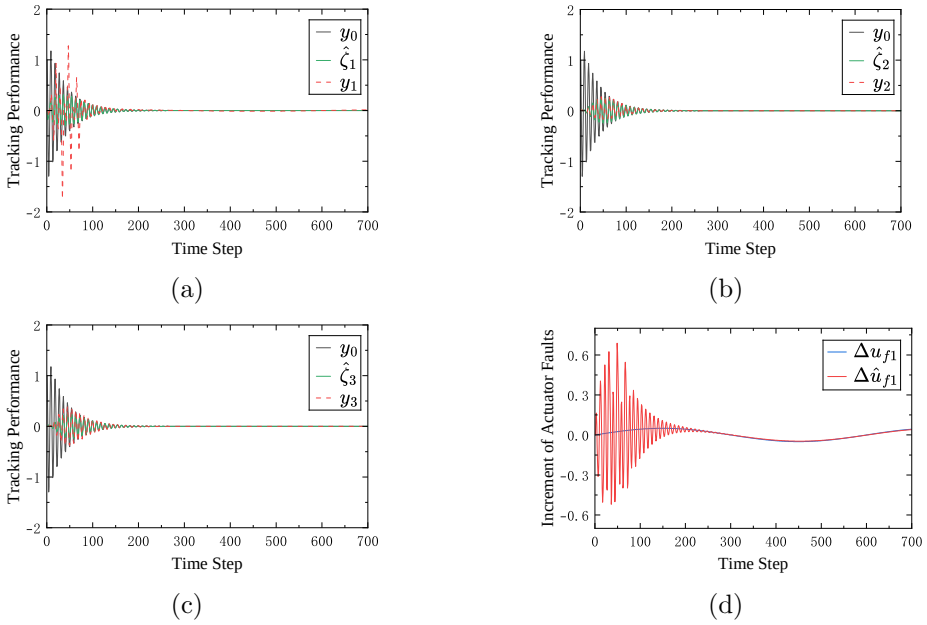

Figure 5: Performance of followers and adaptive actuator estimator under the proposed control algorithm. (a),(b) and (c) are the tracking performances of Follower 1, Follower 2, and Follower 3, respectively. (d) is the performance of the adaptive actuator estimator.

To demonstrate the effectiveness of the proposed algorithm, its performance is compared with the MFAC-based control algorithm incorporating fault estimation, as presented in [23]. The tracking performance and actuator fault estimation results are illustrated in Figure 6. As shown in Figures 6(a), 6(b), and 6(c), the followers fail to accurately track the leader's trajectory under the control strategy of [23], despite the presence of fault estimation. This suggests limitations in the controller's ability to compensate

for actuator faults in a coordinated manner.

Furthermore, Figure 6(d) indicates that while the adaptive estimator in [23] is capable of identifying the actuator fault increments after the 250th step, the system still fails to maintain consensus. This observation implies that actuator faults in one agent not only impair its own tracking ability but also negatively impact the behavior of other agents in the network, likely due to the coupled nature of the communication topology. These findings highlight the importance of integrating both accurate fault estimation and robust distributed control, as achieved by the proposed algorithm.

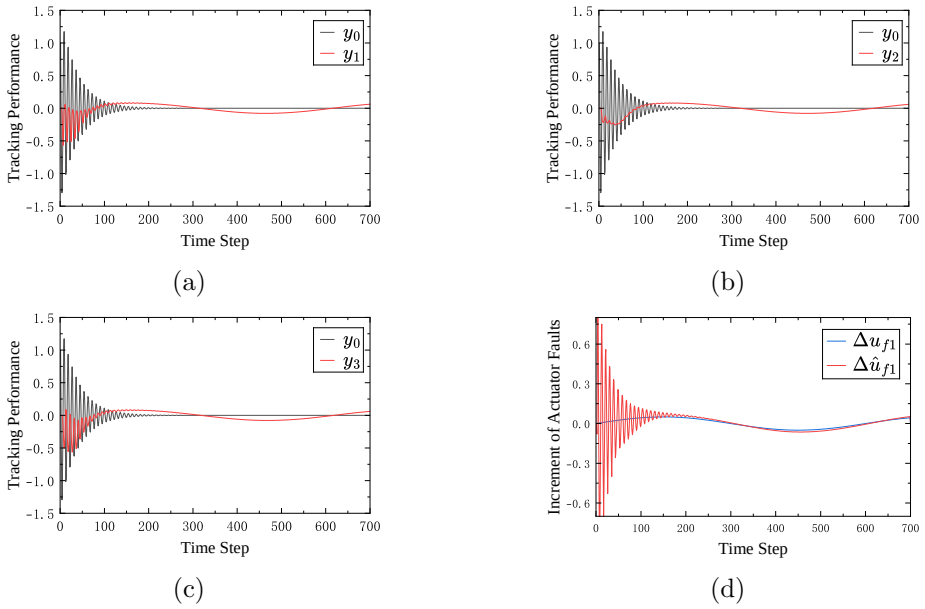

Figure 6: Performance of followers and adaptive actuator estimator under the control algorithm in [23]. (a),(b) and (c) are the tracking performances of Follower 1, Follower 2, and Follower 3, respectively. (d) is the performance of the adaptive actuator estimator.

To further evaluate the effectiveness of the proposed algorithm, four widely used error performance indicators are introduced. The mathematical definitions of these indicators are provided as follows:

$$IAE = \sum_{i=1}^{N}\sum_{s=1}^{T}|e_{Si}(s)| \qquad ISE = \sum_{i=1}^{N}\sum_{s=1}^{T}e_{Si}^2(s)$$

$$ITAE = \sum_{i=1}^{N}\sum_{s=1}^{T}s|e_{Si}(s)| \qquad ITSE = \sum_{i=1}^{N}\sum_{s=1}^{T}se_{Si}^2(s)$$

As shown in Table 1, compared with the algorithm presented in [23], the proposed algorithm achieves reductions of 66.1%, 53.1%, 94.2%, and 86.1% in the IAE, ISE, ITAE, and ITSE indicators, respectively. These substantial improvements across all four performance metrics indicate that the proposed method not only enhances tracking accuracy and dynamic response speed but also significantly mitigates system overshoot and long-term error accumulation. Overall, the results highlight the effectiveness and efficiency of the proposed control strategy in achieving high-performance consensus tracking in heterogeneous MASs.

Table 1: Error Performance Indicators Under Different Algorithms

	The proposed algorithm	The algorithm in [23]
IAE	68.92	203.59
ISE	40.56	86.45
ITAE	2.11e+03	3.69e+05
ITSE	520.09	3.74e+03

5.2. Numerical Simulation 2

Consider a heterogeneous MAS with three followers and one leader, where the leader's output is time-varying and non-convergent. The communication topology and follower dynamics are the same as in Simulation 1.

Denote the dynamics of the leader as:

$$\begin{aligned} x_0(k+1) &= \begin{bmatrix} \cos(0.5\pi/150) & \sin(0.5\pi/150) \\ -\sin(0.5\pi/150) & \cos(0.5\pi/150) \end{bmatrix} x_0(k) \\ y_0(k) &= \begin{bmatrix} 0 & 1 \end{bmatrix} x_0(k). \end{aligned} \tag{33}$$

Moreover, assume the actuator faults occur on follower 1 as $\Delta u_{f1} = 0.15\sin(0.5s\pi/150)$.

The observer parameters are set as $\sigma_i = \upsilon_i = 0.3$, $\kappa_i = 0.4$ for $i = 1, 2, 3$. The adaptive controller parameters are: $m_1 = 0.5$, $\varsigma_1 = \varsigma_2 = 0.99$, $\varsigma_3 = 0.9$, $\alpha_1 = 0.01$, $\alpha_2 = 0.1$, $\alpha_3 = 1$, $\rho_1 = 0.9$, $\rho_2 = 1$, $\rho_3 = 0.1$, $\lambda_1 = 0.04$, $\lambda_2 = 0.01$, $\lambda_3 = 0.1$. Sensor bounds are $\bar{y}_i = 0.2$ for $i = 1, 2, 3$, and initial states are $x_0 = [0.2, -0.2]^{\mathrm{T}}$, $y_1 = y_2 = y_3 = 0$.

The observation errors of the followers are shown in Figures 7 and 8. As seen, the distributed observer accurately estimates the leader's dynamics by

the 30th step and the output by the 120th step, confirming the effectiveness of the proposed observer design.

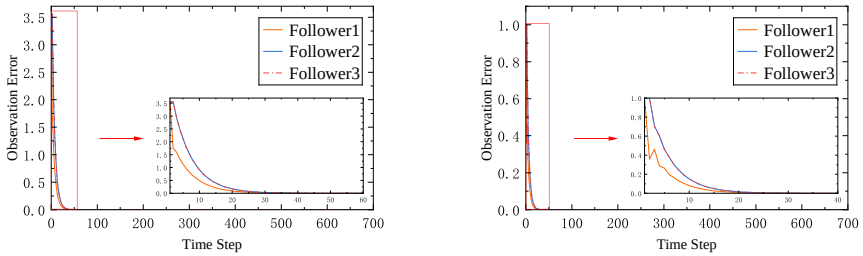

(a) $\|e_{\mathcal{A}i}\|^2 = \|\hat{\mathcal{A}}_i - \mathcal{A}_0\|^2$ (b) $\|e_{\mathcal{C}i}\|^2 = \|\hat{\mathcal{C}}_i - \mathcal{C}_0\|^2$

Figure 7: Observation errors of the followers relative to the dynamics of the leader.

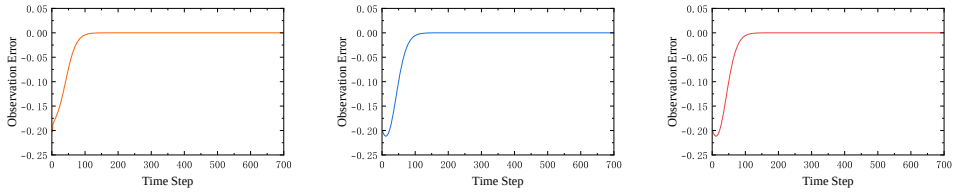

(a) (b) (c)

Figure 8: The followers' observation errors relative to the leader's output. (a)Follower 1 (b)Follower 2 (c)Follower 3

Building on the effectiveness of the distributed observers, the performance of the followers and the adaptive actuator fault estimator is illustrated in Figure 9. Specifically, Figures 9(a), 9(b), and 9(c) show that all three followers successfully track the time-varying output of the leader after approximately the 130th step, despite the heterogeneity in agent dynamics and the presence of actuator faults. This indicates that the proposed control algorithm ensures robust consensus tracking performance even under challenging conditions. In addition, Figure 9(d) demonstrates the performance of the adaptive actuator fault estimator. The estimator is able to accurately identify and compensate for the actuator fault increments starting from the 300th step. The smooth convergence and low estimation error confirm the reliability of the proposed observer. Overall, the hierarchical MFAC-based framework effectively enables fault-tolerant consensus control in heterogeneous MASs.

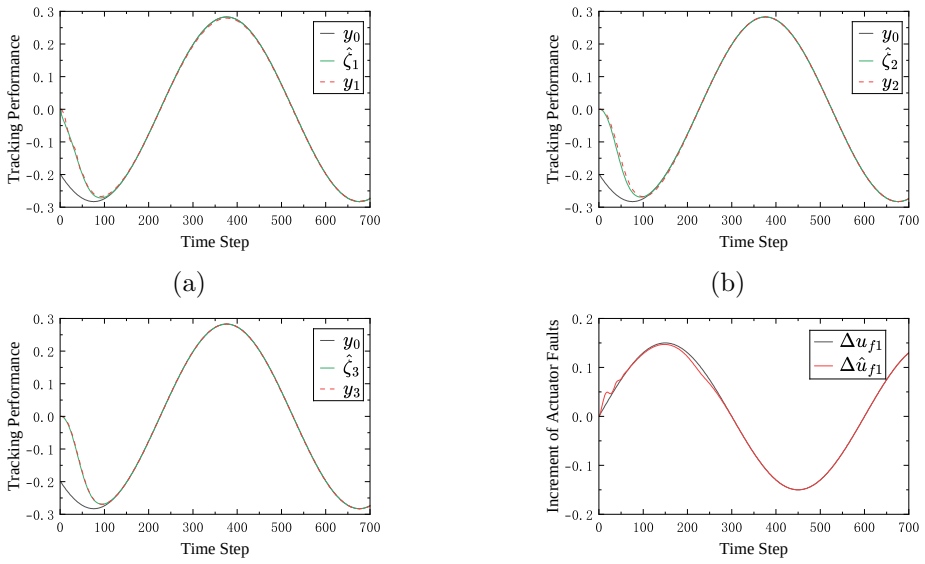

Figure 9: Performance of followers and adaptive actuator estimator under the proposed control algorithm. (a),(b) and (c) are the tracking performances of Follower 1, Follower 2, and Follower 3, respectively. (d) is the performance of the adaptive actuator estimator.

In this subsection, we also compare the performance of the proposed method with the MFAC-based control algorithm without fault estimation, as presented in [23]. The results of this comparison, including tracking performance and actuator fault estimation, are shown in Figure 10. As illustrated in Figures 10(a), 10(b), and 10(c), the followers fail to track the leader's trajectory under the algorithm in [23], indicating inadequate fault tolerance. Moreover, Figure 10(d) shows that the adaptive estimator fails to accurately estimate the actuator faults. The absence of fault compensation consequently prevents the system from maintaining consensus. These observations suggest that, under the control algorithm in [23], actuator faults in a single agent not only impair its own tracking ability but also negatively impact the overall system performance by propagating the effects to other agents.

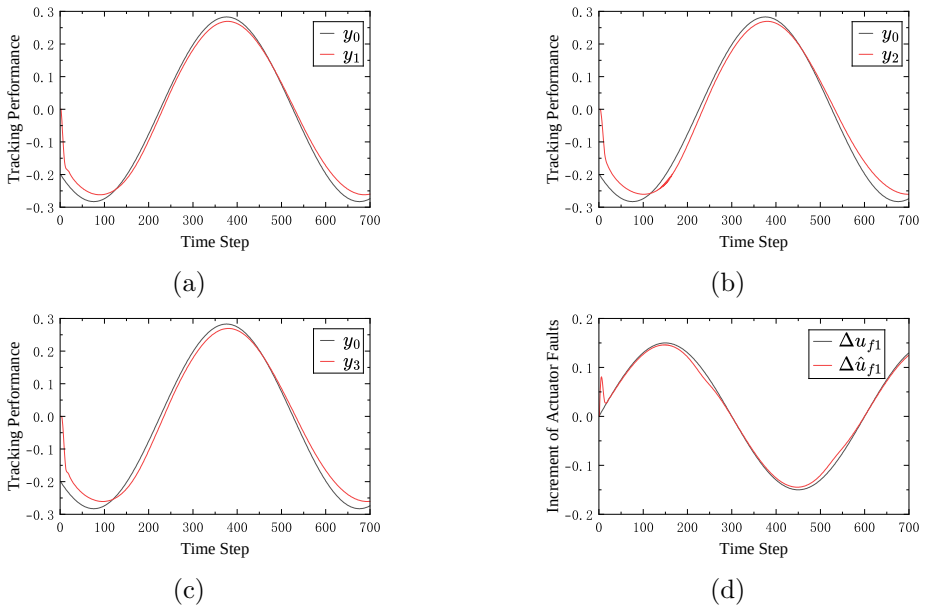

Figure 10: Performance of followers and adaptive actuator estimator under the control algorithm in [23]. (a),(b) and (c) are the tracking performances of Follower 1, Follower 2, and Follower 3, respectively. (d) is the performance of the adaptive actuator estimator.

Table 2: Error Performance Indicators Under Different Algorithms

	The proposed algorithm	The algorithm in [23]
IAE	30.61	38.53
ISE	3.66	1.36
ITAE	2.21e+03	1.18e+04
ITSE	79.13	235.55

Similarly, Table 2 compares the proposed algorithm with [23] using four performance metrics. The proposed method reduces IAE, ITAE, and ITSE by 20.1%, 81.3%, and 66.4%, respectively. While its ISE is slightly higher, the lower ITSE reflects better long-term stability. This suggests that although minor initial fluctuations may occur, the proposed controller stabilizes rapidly, whereas [23] exhibits sustained oscillations. Overall, the proposed algorithm achieves higher tracking accuracy, faster response, and improved control stability.

5.3. Multiple Manipulators Control Simulation

In this subsection, a MAS consisting of four DC motor-driven single-link manipulators [32] is considered, with their dynamics described as follows:

$$J_i\ddot{\theta}_i + f_i\dot{\theta} + (\frac{1}{2}m_i + M_i)gl_i\sin(\theta_i) = u_i \tag{34}$$

where θ_i, $\dot{\theta}_i$, and $\ddot{\theta}_i$ denote the angular displacement, velocity, and acceleration of the ith manipulator, respectively. u_i denotes the control input applied to the manipulator. The moment of inertia J_i is defined as $J_i = M_i l_i^2 + \frac{1}{3}m_i l_i^2$ and the gravitational acceleration is $g = 9.8m/s^2$, for $i = 1, 2, 3, 4$.

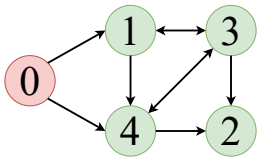

Figure 11: The communication graph of the multiple manipulator control simulation

The communication graph of this simulation is shown in Figure 11. Moreover, the dynamics of the leader in this simulation are denoted as the same way as in the numerical simulation 2. Moreover, assume the actuator faults occur on follower 1 as $\Delta u_{f1} = 0.25\sin(0.5s\pi/125)$.

The observer parameters are set as same as in the numerical simulation 2. The adaptive controller parameters are: $m_1 = 0.55$, $\varsigma_1 = 0.55$, $\varsigma_{2,3,4} = 0.99$, $\alpha_1 = 0.01$, $\alpha_2 = 0.01$, $\alpha_3 = 0.001$, $\alpha_4 = 0.1$, $\rho_1 = 0.1$, $\rho_2 = 0.1$, $\rho_3 = 0.1$, $\rho_4 = 0.1$, and $\lambda_1 = 0.1$, $\lambda_2 = 1.5$, $\lambda_3 = 1.5$, $\lambda_4 = 1.5$. Sensor bounds are set as $\bar{y}_i = 0.3$ for $i = 1, 2, 3, 4$, and the initial states are $x_0 = [0.2, -0.2]^{\mathrm{T}}$, $y_{1,2,3,4} = 0$. The follower dynamics parameters are: $m_1 = 1$, $M_1 = 2$; $m_2 = 1.1$, $M_2 = 2$; $m_3 = 1$, $M_3 = 1.9$; $m_4 = 0.9$, $M_4 = 1.8$; and $l_{1,2,3,4} = 0.5$.

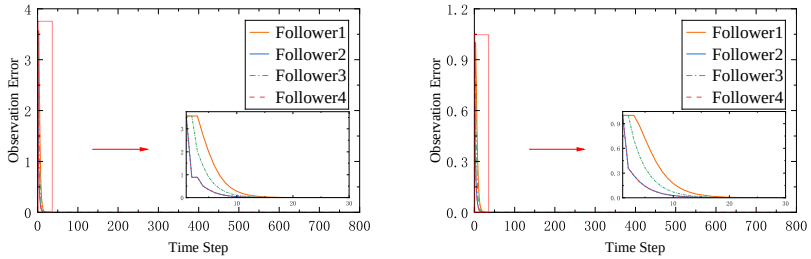

(a) $\|e_{\mathcal{A}i}\|^2 = \|\hat{\mathcal{A}}_i - \mathcal{A}_0\|^2$ (b) $\|e_{\mathcal{C}i}\|^2 = \|\hat{\mathcal{C}}_i - \mathcal{C}_0\|^2$

Figure 12: Observation errors of the followers relative to the dynamics of the leader.

Figures 12 and 13 depict the followers' observation errors for the leader's dynamics and output, respectively. The observer accurately estimates the dynamics by the 25th step and the output by the 75th step, validating its effectiveness in practice.

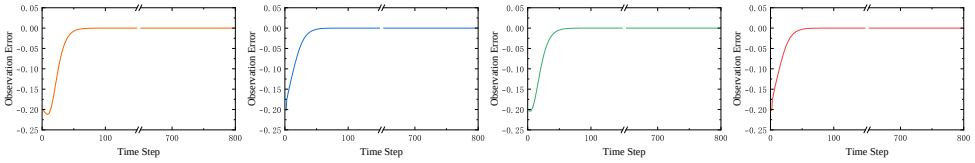

(a) (b) (c) (d)

Figure 13: The followers' observation errors relative to the leader's output. (a)Follower 1 (b)Follower 2 (c)Follower 3 (d)Follower 4

Building on the effectiveness of the distributed observers, the performance of the followers and the adaptive actuator fault estimator is illustrated in Figure 14 and Figure 15, respectively. As shown in Figure 14, the followers achieve successful tracking of the leader's output after the 100th step, despite the presence of hybrid faults. Additionally, Figure 15 demonstrates that the adaptive fault estimator accurately identifies the actuator fault increments after the 300th step.

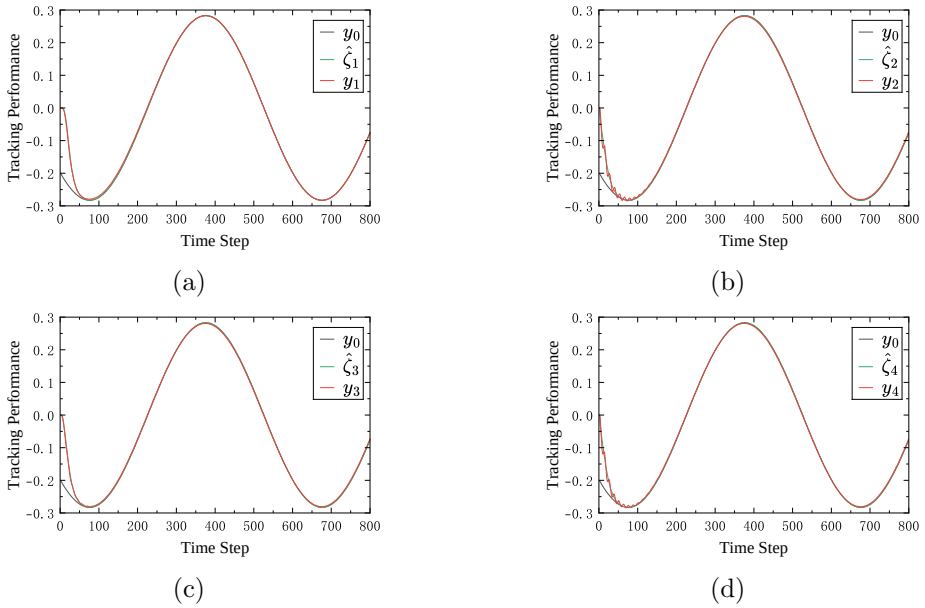

(a) (b) (c) (d)

Figure 14: Tracking performance of the followers under the proposed control algorithm. (a)Follower 1 (b)Follower 2 (c)Follower 3 (d)Follower 4.

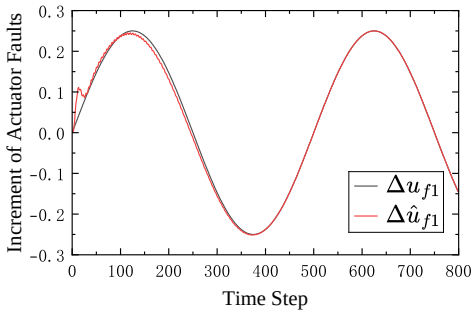

Figure 15: The performance of the adaptive actuator estimator.

These results confirm the practical effectiveness of the proposed hierarchical data-driven safety control algorithm. Through real-time observation, adaptive fault estimation, and robust consensus tracking, it demonstrates strong applicability to heterogeneous MASs under mixed fault conditions.

6. Conclusion

In this paper, we propose a distributed data-driven security control algorithm for unknown nonlinear MASs with actuator faults and sensor saturation. A hierarchical framework was introduced to eliminate reliance on consensus errors, enabling structural decoupling. Within this framework, an online observer estimates the leader's dynamics and state, guiding the design of a distributed MFAC-based controller to achieve accurate consensus tracking under hybrid faults. Simulation results confirm the algorithm's effectiveness and robustness for practical deployment in heterogeneous MASs. Future work will address challenges such as performance guarantees, input/output constraints, and communication limitations to enhance the method's applicability in real-world scenarios.

7. Declaration of competing interest

The authors declare that they have no known competing financial interests or personal relationships that could have appeared to influence the work reported in this paper. In addition, this paper represents original work that has not been published previously and is not currently under consideration for publication elsewhere in any form.

References

[1] L. Zhou, P. Tokekar, Multi-robot coordination and planning in uncertain and adversarial environments, Current Robotics Reports 2 (2021) 147–157.

[2] Z. Chang, G. Zong, W. Wang, M. Yue, X. Zhao, Formation control and obstacle avoidance design for networked usv swarm with exogenous disturbance under intermittent communication, IEEE Transactions on Network Science and Engineering (2025).

[3] J. Luo, Y. Yang, Z. Wang, Y. Chen, Localization algorithm for underwater sensor network: A review, IEEE Internet of Things Journal 8 (17) (2021) 13126–13144.

[4] T. Shi, F. Zhu, Security time-varying formation control for multi-agent systems under denial-of-service attacks via unknown input observer, IEEE Transactions on Network Science and Engineering 10 (4) (2023) 2372–2385.

[5] Z. Yu, W. Zhang, Event-triggered secure control for consensus of the discrete-time multiagent system against complex cooperative attacks, IEEE Transactions on Systems, Man, and Cybernetics: Systems (2024).

[6] Z. Hou, S. Xiong, On model-free adaptive control and its stability analysis, IEEE Transactions on Automatic Control 64 (11) (2019) 4555–4569.

[7] B.-F. Yue, M.-Y. Su, X.-Z. Jin, W.-W. Che, Event-triggered mfac of nonlinear ncss against sensor faults and dos attacks, IEEE Transactions on Circuits and Systems II: Express Briefs 69 (11) (2022) 4409–4413.

[8] Q. Zhou, Q. Ren, H. Ma, G. Chen, H. Li, Model-free adaptive control for nonlinear systems under dynamic sparse attacks and measurement disturbances, IEEE Transactions on Circuits and Systems I: Regular Papers (2024).

[9] F. Li, Z. Hou, Learning-based model-free adaptive control for nonlinear discrete-time networked control systems under hybrid cyber attacks, IEEE Transactions on Cybernetics 54 (3) (2022) 1560–1570.

[10] C. Yang, T. Zheng, M. Bu, P. Li, J. M. Guerrero, Distributed model-free adaptive control strategy for hybrid ac/dc microgrid with event-triggered mechanism, IEEE Transactions on Industrial Electronics 71 (8) (2023) 9077–9086.

[11] S. Guo, Y. Pan, H. Li, L. Cao, Dynamic event-driven adp for n-player nonzero-sum games of constrained nonlinear systems, IEEE Transactions on Automation Science and Engineering 22 (2025) 7657–7669.

[12] Y. Zhang, M. Chadli, Z. Xiang, Prescribed-time formation control for a class of multiagent systems via fuzzy reinforcement learning, IEEE Transactions on Fuzzy Systems 31 (12) (2023) 4195–4204.

[13] Q. Shen, P. Shi, J. Zhu, S. Wang, Y. Shi, Neural networks-based distributed adaptive control of nonlinear multiagent systems, IEEE Transactions on Neural Networks and Learning Systems 31 (3) (2019) 1010–1021.

[14] F. Li, Z. Hou, Controller-dynamic-linearization-based distributed model-free adaptive control for nonlinear multiagent systems, IEEE Transactions on Systems, Man, and Cybernetics: Systems 54 (2) (2023) 985–996.

[15] Y. Sun, X. Chen, W. Wang, H. Fu, M. Wu, Model-free output consensus control for partially observable heterogeneous multivehicle systems, IEEE Internet of Things Journal 7 (8) (2020) 7135–7147.

[16] W. Wang, X. Chen, H. Fu, M. Wu, Model-free distributed consensus control based on actor–critic framework for discrete-time nonlinear multiagent systems, IEEE Transactions on Systems, Man, and Cybernetics: Systems 50 (11) (2018) 4123–4134.

[17] X. Bu, Z. Hou, H. Zhang, Data-driven multiagent systems consensus tracking using model free adaptive control, IEEE Transactions on Neural Networks and Learning Systems 29 (5) (2018) 1514–1524.

[18] J. Liang, X. Bu, L. Cui, Z. Hou, Event-triggered asymmetric bipartite consensus tracking for nonlinear multi-agent systems based on model-free adaptive control, IEEE/CAA Journal of Automatica Sinica 10 (3) (2023) 662–672.

[19] S. S. A. Sahafi, M. M. Farsangi, Fully distributed data-driven model-free adaptive control for consensus tracking in multi-agent systems, ISA transactions (2025).

[20] H. Zhao, L. Peng, H. Yu, Model-free adaptive consensus tracking control for unknown nonlinear multi-agent systems with sensor saturation, International Journal of Robust and Nonlinear Control 31 (13) (2021) 6473–6491.

[21] T. Liu, Z. Hou, Model-free adaptive containment control for unknown multi-input multi-output nonlinear mass with output saturation, IEEE Transactions on Circuits and Systems I: Regular Papers 70 (5) (2023) 2156–2166.

[22] S. Xiong, Z. Hou, Data-driven formation control for unknown mimo nonlinear discrete-time multi-agent systems with sensor fault, IEEE transactions on neural networks and learning systems 33 (12) (2021) 7728–7742.

[23] Y. Wang, Z. Wang, Distributed model free adaptive fault-tolerant consensus tracking control for multiagent systems with actuator faults, Information Sciences 664 (2024) 120313.

[24] M. Hu, L. Bu, Y. Bian, H. Qin, N. Sun, D. Cao, Z. Zhong, Hierarchical cooperative control of connected vehicles: From heterogeneous parameters to heterogeneous structures, IEEE/CAA Journal of Automatica Sinica 9 (9) (2022) 1590–1602.

[25] L. Xia, Q. Li, R. Song, S. S. Ge, Distributed optimized dynamic event-triggered control for unknown heterogeneous nonlinear mass with input-constrained, Neural Networks 154 (2022) 1–12.

[26] J. Sun, Z. Ming, Cooperative differential game-based distributed optimal synchronization control of heterogeneous nonlinear multiagent systems, IEEE Transactions on Cybernetics (2023).

[27] D. Wang, L. Hu, X. Li, J. Qiao, Online fault-tolerant tracking control with adaptive critic for nonaffine nonlinear systems, IEEE/CAA Journal of Automatica Sinica 12 (1) (2025) 215–227.

[28] S. Xiong, Z. Hou, Data-driven formation control for unknown mimo nonlinear discrete-time multi-agent systems with sensor fault, IEEE Transactions on Neural Networks and Learning Systems 33 (12) (2022) 7728–7742.

[29] C. Chen, F. L. Lewis, K. Xie, S. Xie, Y. Liu, Off-policy learning for adaptive optimal output synchronization of heterogeneous multi-agent systems, Automatica 119 (2020) 109081.

[30] C. Chen, F. L. Lewis, K. Xie, Y. Lyu, S. Xie, Distributed output data-driven optimal robust synchronization of heterogeneous multi-agent systems, Automatica 153 (2023) 111030.

[31] J. Huang, The cooperative output regulation problem of discrete-time linear multi-agent systems by the adaptive distributed observer, IEEE Transactions on Automatic Control 62 (4) (2017) 1979–1984.

[32] R. Chi, Y. Hui, B. Huang, Z. Hou, X. Bu, Data-driven adaptive consensus learning from network topologies, IEEE Transactions on Neural Networks and Learning Systems 33 (8) (2022) 3487–3497.